Smart Structures and Systems, *Vol. 27, No. 3 (2021) 537-546*
DOI: https://doi.org/10.12989/sss.2021.27.3.537

Computer vision-based displacement measurement with m-sequence target

Yi-ding Hu [1], Qi Xia*[2], Rong-rong Hou [3], Yong Xia [3] and Jian-yi Yan [1]

[1] *Faculty of Intelligent Manufacturing, Wuyi University, Jiangmen 529020, China*
[2] *School of Civil Engineering, Southeast University, Nanjing, China*
[3] *Department of Civil and Environmental Engineering, The Hong Kong Polytechnic University, Hong Kong, China*

(*Received January 9, 2020, Revised January 5, 2021, Accepted January 5, 2021*)

Abstract. The development of image sensors enables the application of vision-based techniques to the non-contact displacement measurement of large-scale structures. The features of the physical targets are critical to the accuracy, stability and anti-interference of the displacement measurement results. In this study, a novel m-sequence target and the associated circular correlation processing technique are developed for real-time displacement measurement. The properties of the m-sequence as a pseudo-random sequence are introduced. The vision-based displacement calculation method is then derived from the correlation property of the m-sequence. The algorithms and measurement systems are integrated in the LabVIEW environment. To verify the anti-interference performance of the developed system, static and dynamic experimental tests are carried out with various forms of interference, such as partial occlusion, uneven illumination, out of focus and smoke effect. Experimental results indicate that the developed system cannot only accurately measure structural displacement, but also has outstanding anti-interference performance, even if 30% of the target is masked.

Keywords: computer vision; m-sequence; displacement measurement; target tracking; structural health monitoring

1. Introduction

Structural health monitoring (SHM) aims at providing valuable information for condition assessment and decision making of maintenance through measurement of structural loadings and/or responses (Brownjohn 2006, Ou and Li 2010, Koo *et al*. 2013, Xia *et al*. 2017, 2020). Structural deformation is an essential metric of such purpose because it is directly related to the structural stiffness (Yi *et al*. 2013, Xia *et al*. 2014, Hu *et al*. 2019). Excessive deformation will not only affect the structural serviceability but also accelerate its degradation.

Traditional displacement sensors such as the linear variable differential transformers (Li and Hao 2016) are convenient to be used in laboratories but not on a real-life structure for several reasons, for example, a stable platform near the measurement points is required to install the sensors; in addition, the measurement stroke is limited. Advanced sensors such as Global Position System (GPS), Interferometric Radar, and Laser Doppler Vibrometer (Kim *et al*. 2016) have been developed and applied for displacement measurement in recent decades. However, the accuracy of GPS is not sufficient and the sampling rate not high for SHM. Although radar- and laser-based systems provide high precision, the high costs hinder their wide applications in practice.

In this regard, the computer vision-based measurement techniques offer a significant potential for displacement monitoring of structures (Feng and Feng 2018, Bao *et al*. 2019, Casciati *et al*. 2019, Jung *et al*. 2019, Spencer *et al*. 2019), such as of high-rise buildings (Lee *et al*. 2012, Chen *et al*. 2017), short-span bridges (Catbas *et al*. 2012, Feng *et al*. 2015, Xu *et al*. 2018) and long-span bridges (Jeon *et al*. 2011, Zhou *et al*. 2012, Ye *et al*. 2013). Most of the techniques are developed based on one or several image targets in a black and white plan with a specific geometric shape, which is convenient for the camera to capture and locate. Then, the displacement of the structure is determined by calculating the number of moving pixels of the geometric boundary.

Despite that the existing vision-based techniques have received successes in measuring vibration displacements of the experimental and in-field structures, two main shortcomings exist. First, these techniques usually require some complicated algorithms to process the image information**.** The techniques are primarily enabled by the template matching/registration techniques, including pattern matching (Ye *et al*. 2013), edge detection, digital image correlation (Busca *et al*. 2015), Hough transforms (Song *et al*. 2014), the optical flow-based method (Caetano *et al*. 2011), the upsampled cross-correlation, orientation code matching (Feng and Feng 2016), Lucas-Kanade template tracking (Guo and Zhu 2016), multi-object tracking (Ye *et al*. 2016a) and so on. Lately, efforts have been made to eliminate the target panel and significantly improve the convenience of testing (Khuc and Catbas 2017, Kuddus *et al*. 2019), but there are still many problems for the accuracy and robustness of measurement (Ribeiro *et al*. 2014, Yoon *et al*. 2016). Most importantly, the natural targets cannot be used for the long-term monitoring of structural displacement due to its stability. So, the existing computer vision-

*Corresponding author, Assistant Professor,
E-mail: qixia@seu.edu.cn

ISSN: 1738-1584 (Print), 1738-1991 (Online)

based measurement techniques based on complex algorithms are difficult for engineers to learn and apply.

The other drawback is that the traditional vision-based displacement measurements are not robust in anti-interference and subject to negative influence of environmental factors, such as light intensity, air refraction, shielding, focusing, etc. For example, Olaszek (1999) found that the air turbulence has a more significant influence on the short-term displacement measurement. Correlation-based template matching is not robust to this effect apart from testing during overcast weather, while the feature point matching method was reported to be less sensitive (Ehrhart and Lienhart 2015). The influence of lighting variations might be reduced by enabling camera auto-exposure settings (Xu *et al*. 2018). Lee *et al*. (2017) presented a vision-based displacement measurement approach tailored to a field-testing environment with enhanced robustness to intense sunlight. Ye *et al*. (2016b) conducted a series of experiments on a shaking table and demonstrated that illumination and vapor have a critical effect on the measurement results. Therefore, improving the robustness and anti-interference is critical to the success of the vision-based displacement measurement techniques.

In this connection, a novel pseudo-random sequence based measurement technology is developed in this article. The pseudo-random sequence is a regular periodical binary sequence though looking like a noise one. m-sequence, or maximal length sequence of linear feedback shift register, is the most important and fundamental one (Peterson *et al*. 1995). Its most important property is the impulse-like autocorrelation functions. In addition, it has many statistical properties with white noise despite being entirely deterministic and can be generated very quickly by the use of the shift-registers. Accordingly, this coding technique dramatically simplifies the image post-processing algorithm. Meanwhile, the anti-interference performance of the barcode target can be significantly improved by the autocorrelation property of the m-sequence.

This article is organized as follows: First, the computer vision-based displacement measurement system with the m-sequence target is introduced briefly. Second, the m-sequence coding technique and its autocorrelation theory are deduced in detail. Next, the displacement measurement techniques are integrated into the LabVIEW platform. The accuracy and anti-interference are verified in the laboratory. The conclusions are finally drawn.

2. The framework of vision-based displacement measurement

The computer vision-based displacement measurement developed in this study contains an industrial camera, optical lens, m-sequence target, data acquisition and processing software, which are introduced as follows.

The specific m-sequence target with coding and size information is designed and fixed to the structure as shown in Fig. 1. When the structure has vertical vibration, the m-sequence target will also move with it. The industrial camera captures the video of the target image at a fixed frame rate. Then, the binary coded information of each frame is processed in real-time and the circular cross-correlation calculation with the local m-sequence is calculated. The relative positions of the two cross-correlation peaks correspond to the relative displacement of the two frames at intervals. Finally, the dynamic displacement of the structure can be obtained by combining all the relative displacements. Since the correlation property

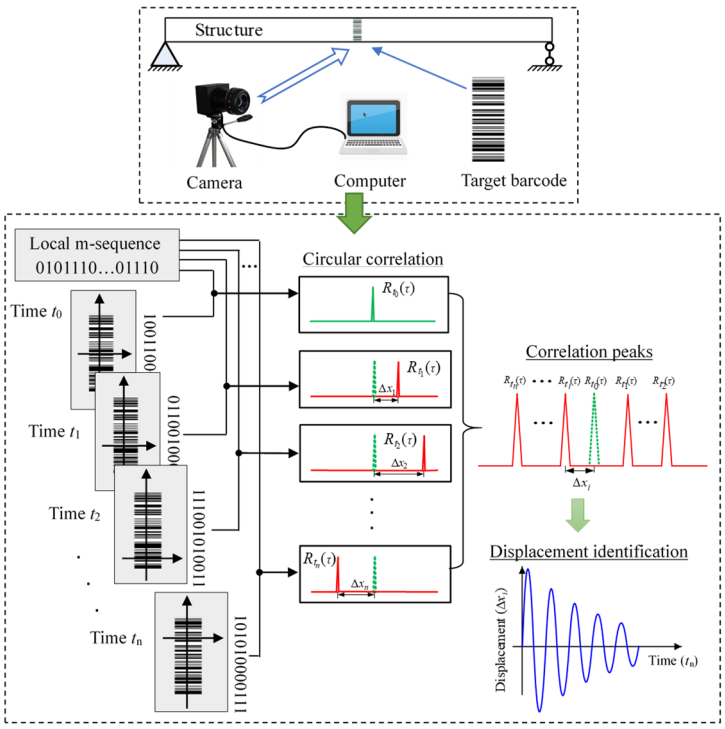

Fig. 1 The schematic of computer vision-based displacement measurement with m-sequence target

of the m-sequence carries the displacement information of the structure, the anti-interference ability of the vision-based displacement measurement system will be significantly improved.

3. m-sequence coding technique and its autocorrelation property

A pseudo-random sequence is a periodic binary sequence with a noiselike waveform that is usually generated utilizing a feedback shift register, which consists of an ordinary shift register made up of k flip-flops (two-state memory stages) and a logic circuit that is interconnected to form a feedback circuit. Note that the "all zeros state" of the shift register never occurs. As a result, the pseudo-random sequence produced by a linear feedback shift register with k flip-flops cannot exceed $2^k - 1$. In fact, every linear feedback shift register with the maximum cycle length (which is $2^k - 1$, where k is the length of the linear feedback shift register) may be built from a primitive polynomial of degree k over Galois Field (2), or GF(2) (Peterson *et al*. 1995) in short. So, when the period is precisely $2^k - 1$, the pseudo-random sequence is called a maximal-length-sequence or simply m-sequence.

The m-sequence has some characteristics of white noise. The most important property is the impulse-like autocorrelation functions. The normalized (by the length of the sequence) autocorrelation of a genuinely random process will have a single peak equal to 1.0 only at the zero offset point and virtually zero everywhere else. Each bit in the m-sequence is also called a chip. If we convert the values of the chips in the m-sequence 0 to 1 and 1 to −1 and perform "circular correlation" of the m-sequence, the normalized autocorrelation of the m-sequence can be obtained as

$$R_{xx}(\tau) = \frac{1}{N}\sum_{i=1}^{N} x\{rem[(i+\tau), N]\} \cdot x(i) \qquad (1)$$

where $x(i)$ $(i = 1,2,\cdots N)$ is an m-sequence with N-length, and $rem[(i+\tau), N]$ represents the remainder of taking N for $i + \tau$.

The normalized autocorrelation of an m-sequence with N-length will also has a peak equal to 1.0 at the zero offset point, and will drop linearly to a very low constant value (equal to $-1/N$) at $\pm T_c$ on either side of that peak (whereT_c is the time duration of one chip) (Welch *et al*. 2011) as shown in Fig. 2. The autocorrelation peak of the m-sequence is sharp and large (maximal) upon synchronization (i.e., for time shift equal to zero) and is minimal (very close to zero) for any time shift different than zero. This confirms that the m-sequence have the best periodic autocorrelation, and has powerful anti-interference performance. The fact that any timing offset more than $\pm 0.5T_c$ from an integer value of T_c will result in a very low constant autocorrelation, which is equal to $-1/N$. Note that for the very long sequences, the $-1/N$ term is approximately zero, and the autocorrelation peaks are spaced so far apart that it appears to be very much like random noise. On the other hand, Fig. 2 illustrates that the longer the m-sequence length N, the larger the gain of correlation peak and hence the more resistance to noise and interference. Consequently, the m-sequence has a strong anti-interference ability, even in a low signal noise ratio condition. Based on this theoretical property, it will perform displacement measurement based on the m-sequence target.

4. Implementation of the vision-based displacement measurement with the m-sequence target

The procedures of the real-time computer vision-based displacement measurement with the m-sequence target are described as follows:

Step 1: Target design

First, specify the primitive polynomial of k degree determines the k-stage shift register's feedback connections. An N-chip of m-sequence can be generated by MATLAB, where N represents the number of chips in one cycle and is equal to $2^k - 1$. The m-sequence is defined as $x(i)$ ($i = 1, 2,..., N$). To ensure that the lens always captures the target and the displacement of the structure will not exceed the range of the target, the length of the target is designed as a repeating two identical m-sequences. The final sequence length is $2N$. And then, the final sequence is injected into the barcode image as shown in Fig. 3. The middle portion of the target is a barcode corresponding to the m-sequence, where black stripes indicate the code "0" and white stripes indicate "1". Besides, a bold black line is added between the two m-sequences to facilitate the lens to focus on the barcode. For the region of interest (ROI) selection in Step 2, the boundary lines added on the target ensure that the information included in ROI represents N-length chips.

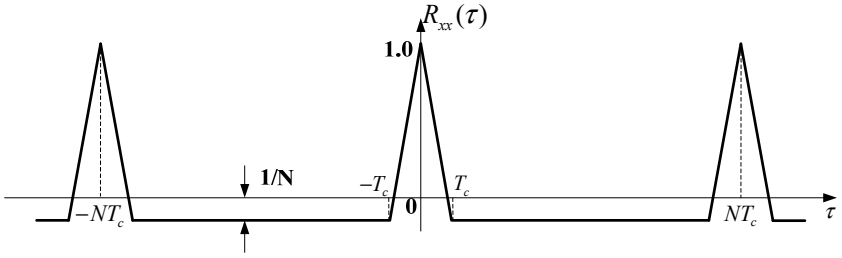

Fig. 2 The autocorrelation curve of m-sequence

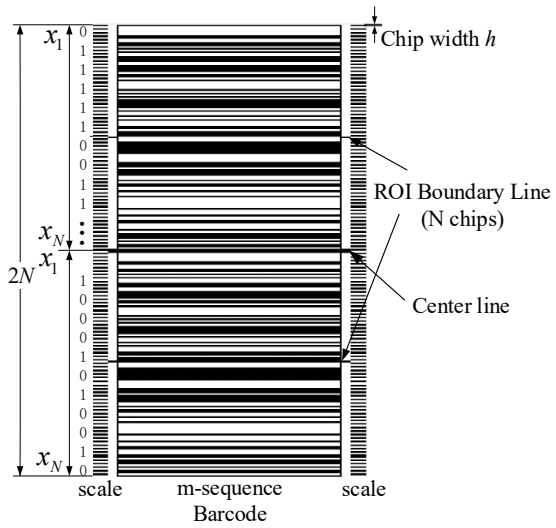

Fig. 3 A target barcode

The design target of the m-sequence has scale information. The equally spaced black lines on both sides are the reference scale, indicating that the image height of each chip of the barcode is h. The size of h corresponds to the printing accuracy of the barcode. In the sequence correlation calculation, the minimum resolution of the correlation peak shift is the spacing of two chips. Therefore, the theoretical accuracy measured by this method is $\pm h$. If the measurement accuracy needs to be improved, the height h of each chip can be reduced. On the other hand, the most suitable focal length of the camera can be determined by seeing the chips clearly.

Step 2: ROI selection

A ROI is a portion of an image that you want to filter or operate on in some way. The focal length of the camera is adjusted to focus on the target center. The ROI is precisely aligned with a cycle-length barcode through the boundary lines. The image A (U×V) of ROI is shown in Fig. 4. If the ROI is set to U×V pixels, every d = U/N pixels mean one chip information of the m-sequence. It is not necessary condition for the camera being perpendicular to the barcode. Because the absolute displacement information already exists in the m-sequence code, the acquisition of m-sequence information in the ROI image has the minimal influence by the horizontal or elevation angle within a larger range.

Step 3: Information acquisition

This study is deploying a LabVIEW based controller for video capture and information acquisition of targets. Video slips of the ROI area is captured by an industrial camera. Each frame of the images is sequentially processed for greying and binarization by the Otsu algorithm (Otsu 1979) in real-time. When a binary image A (U×V) is obtained, an arbitrary column of the data B (U×1) is taken from the middle portion of the binary image. And then, the column data B (U×1) is converted to "0" and "1". As described in Step 2, each chip contains d pixels. So, the new binary code is extracted from every d interval in B and forms the sequence $y_i\,(i=1,2,...,N)$. For subsequent correlation calculations, "0" is converted to "−1" in sequence y_i.

Step 4: The circular correlation algorithm

Due to the periodicity of the m-sequence, the circular algorithm can be used to calculate the correlation between x_i and y_i as shown in Fig. 5. The normalised correlation of x_i and y_i can be expressed as

$$R_{xy}(\tau)=\frac{1}{N}\sum_{i=1}^{N}x\{rem[(i+\tau),N]\}\cdot y(i) \qquad (2)$$

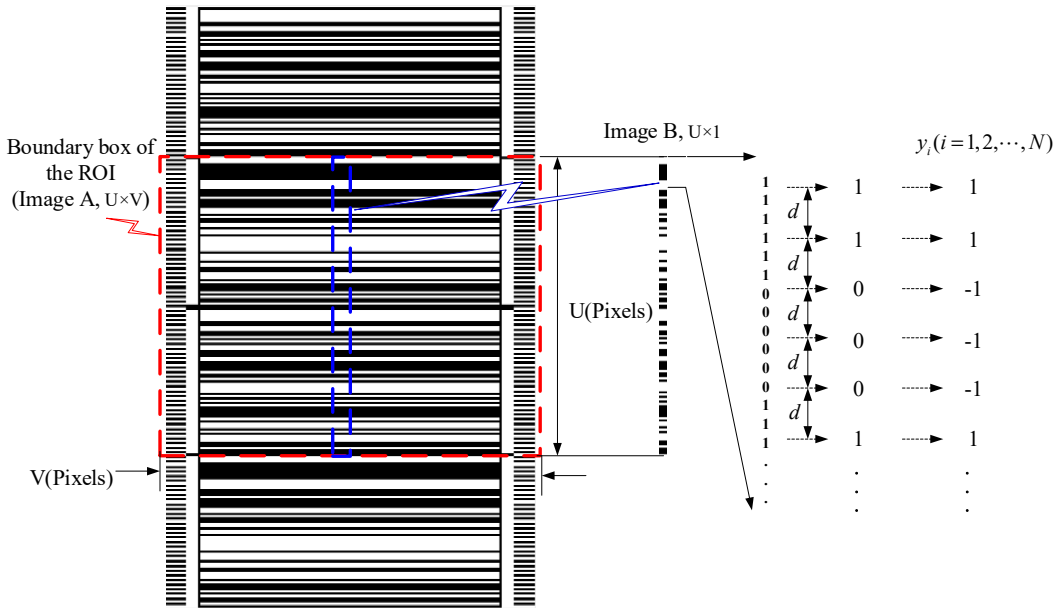

Fig. 4 ROI selection and information acquisition.

where $x_i = [x_1, x_2, \ldots, x_N]$ is the local m-sequence, $y_i = [x_{1+\tau}, x_{2+\tau}, \ldots, x_{N+\tau}]$ is obtained from the column data B (U×1), τ represents the delay of the sequence, and $rem[(i+\tau), N]$ represents the remainder of taking N for $i+\tau$.

A period correlation function $R_{xy}(\tau)$, $(\tau = 0, 1, 2, \ldots, N-1)$ can presented

$$\begin{bmatrix} R_{xy}(0) \\ R_{xy}(1) \\ \vdots \\ R_{xy}(\tau\text{-}1) \\ R_{xy}(\tau) \\ \vdots \\ R_{xy}(N\text{-}1) \end{bmatrix} = \frac{1}{N} \begin{bmatrix} x_1 & x_2 & \cdots & x_{\tau-1} & x_\tau & \cdots & x_{N-1} & x_N \\ x_2 & x_3 & & x_\tau & x_{\tau+1} & & x_N & x_1 \\ & & & \vdots & & & & \\ x_\tau & x_{\tau+1} & \cdots & & \ddots & \cdots & x_{\tau-2} & x_{\tau-1} \\ x_{\tau+1} & x_{\tau+2} & \cdots & & \ddots & \cdots & x_{\tau-1} & x_\tau \\ & & & \vdots & & & & \\ x_N & x_1 & \cdots & x_{\tau-2} & x_{\tau-1} & \cdots & x_{N-2} & x_{N-1} \end{bmatrix} \begin{bmatrix} y_1 \\ y_2 \\ \vdots \\ y_\tau \\ y_{\tau+1} \\ \vdots \\ y_N \end{bmatrix} \tag{3}$$

Assuming that the acquired image has no interference, the correlation function $R_{xy}(\tau)$ has a correlation peak of 1 at τ_0, and others are close to zero as shown in Fig. 5.

Step 5: Displacement calculation

According to Step 4, the correlation peak is automatically recognized for each frame of the image. The initial position of the correlation peak needs to be defined, that is, the original correlation peak $R_{t_0}(\tau)$ of the local sequence and the sequence in the first frame image are shown in Fig. 6. When the target moves, the position of the correlation peak also moves with it together. And then, assume that at time t_i, the correlated peaks $R_{t_i}(\tau)$ moved $\Delta m(t_i)$ chips. At this time, the displacement from the initial position is

$$\Delta x_i = h \times \Delta m(t_i) \tag{4}$$

where $\Delta m(i)$ is chips between the peaks of $R_{t_0}(\tau)$ and $R_{t_i}(\tau)$, and t_i is time point.

The real-time displacement *DIS* is given by

$$DIS = [\Delta x_1, \Delta x_2, \ldots \Delta x_n] \tag{5}$$

After each frame of the image is processed in real-time, the dynamic displacement of the structure can be obtained.

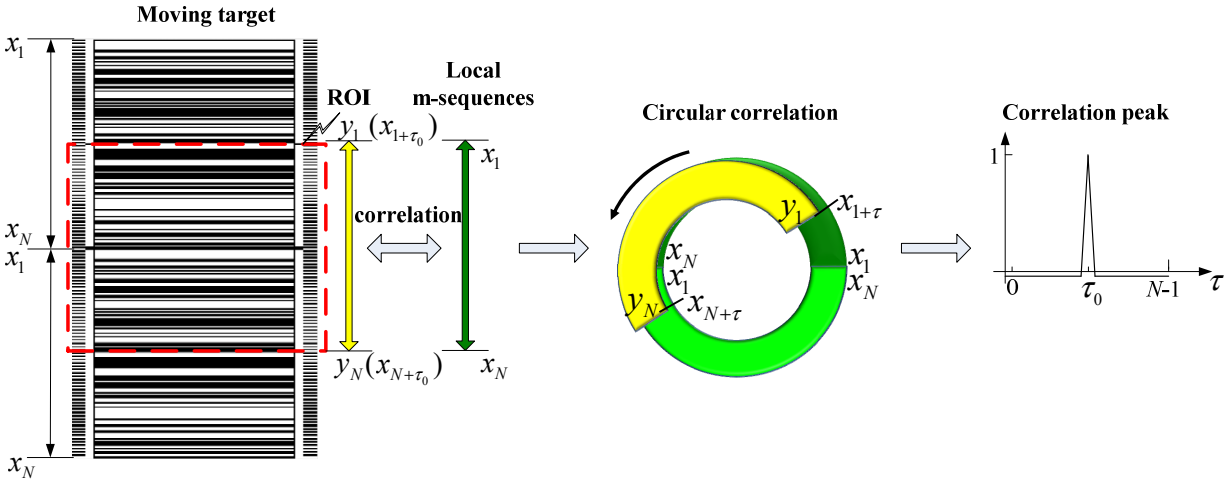

Fig. 5 The circular correlation algorithm

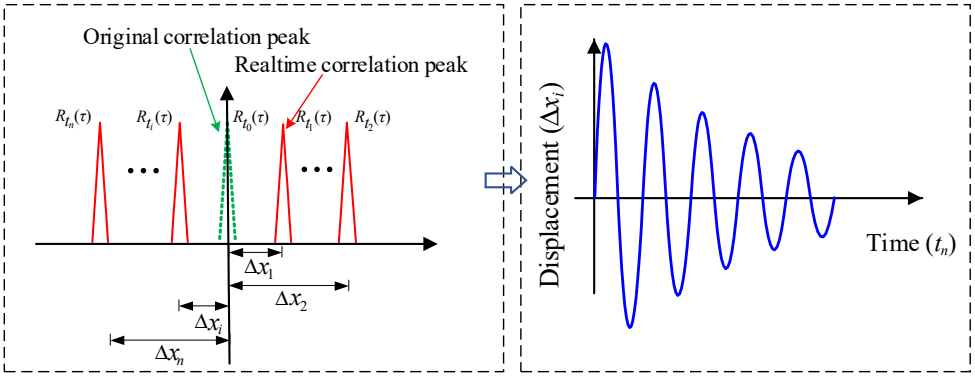

Fig. 6 The displacement calculation

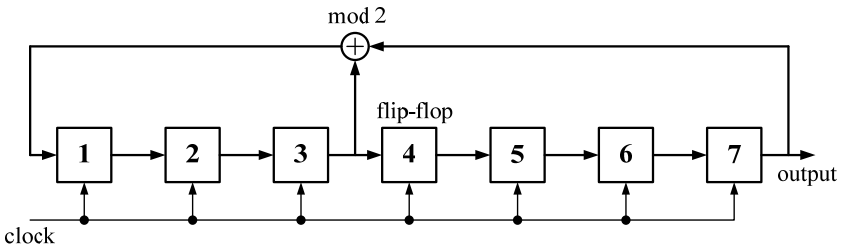

Fig. 7 m-sequence generator with 7 shift registers

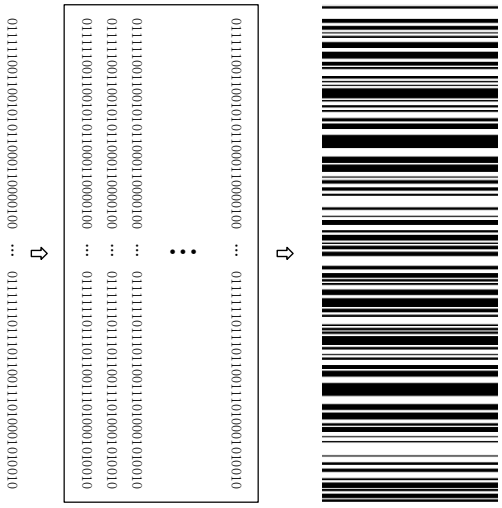

Fig. 8 m-sequence and its barcode image

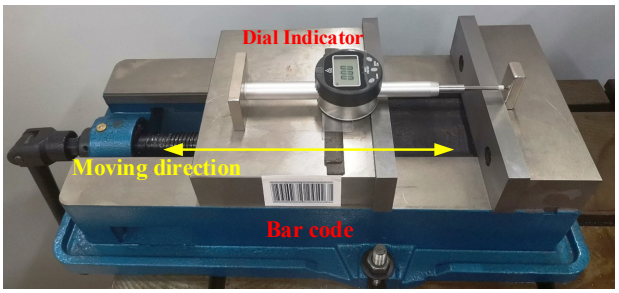

Fig. 9 Details of machine vice

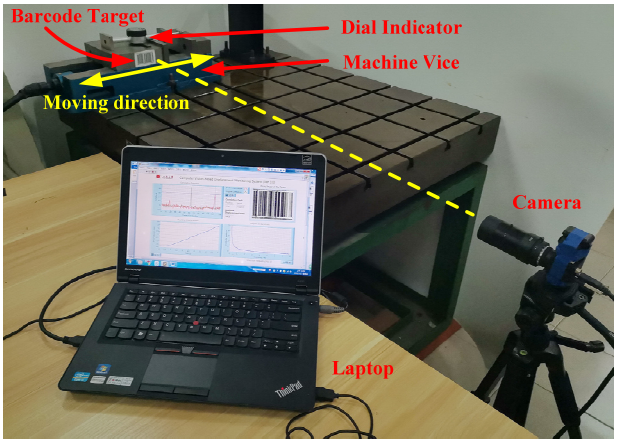

Fig. 10 Experimental setup

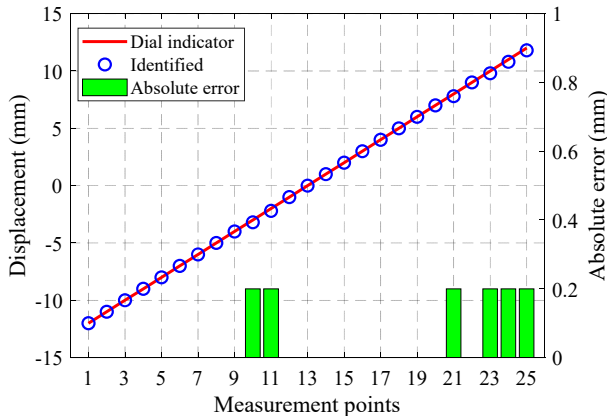

Fig. 11 The comparison of test results

5. System implementation and verification

5.1 Experimental design and system verification

According to Step 1, a binary linear shift-register sequence with a period of $2^7 - 1 = 127$ is adopted in this study, where 7 is the degree of the generator polynomial. The m-sequence generator where $k = 7$ is built as shown in Fig. 7. The 127-chip m-sequence is originated from the primitive polynomial $x^7 + x^3 + 1$ and is arranged into a two-cycle m-sequence column vector. And then, the barcode image data are generated through repeating some copies of the column vector as shown in Fig. 8. The attachments of scale and position information are produced in the barcode target. The print accuracy of each chip is set to $h = 0.2$ mm, indicating that the measurement accuracy is $\pm$ 0.2 mm and the measurement range is $h \times N = 25.4$ mm. Therefore, the full-range error of the system is $(1/127) \times 100 = 0.79\%$. The barcode target image is horizontally installed on the side of a machine vice as shown in Fig. 9. And then, a MindVision® U3B500C industrial camera with a 5-100 mm focal length is fixed at a position approximately 1.2 m from the target. The camera can record videos with maximum 22 frame per second and resolution 2048 × 1536 pixel. The videos are taken by NI-IMAQdx driver software and LabVIEW platform and subsequently transferred to the Laptop. Because the target itself contains size information, the camera does not have to be fully aligned perpendicular to the target. These facilitates of the test system can be rapidly arranged. According to Step 2, the ROI is defined as the length of the 127-chip m-sequence, and the size of the pixel is 1270 × 960. Each chip in the m-sequence will contain 10 pixels. The pixels are

taken out from the middle of ROI, and the chip information of the barcode is extracted according to Step 3. The correlation peaks and their corresponding positions will be obtained by the circular correlation algorithm of Step 4. A laboratory setup of the entire measurement system is shown in Fig. 10.

The proposed system is calibrated and verified using a dial indicator. The initial position is defined, and the dial indicator reading is adjusted to 0. The ROI of the camera is aligned with the centerline of the target image. At this point, the position of the correlation peak is identified by the LabVIEW program, and the displacement of this correlation peak is defined as 0. Next, the target moves left or right by rotating the handle of the machine vice. The readings of the dial indicator and measurement system are recorded for each 1 mm movement of the target image. The comparison results of the measurements are shown in Fig. 11. The results show that the absolute errors of the identification results are less than 0.2 mm. The entire system meets the design requirement.

5.2 Anti-interference performance of static displacement measurement

To verify the anti-interference performance of the proposed measurement method, a series static tests with various forms of interference are carried out.

Case 1 has no interference as shown in Fig. 12. The balanced position is defined, then the barcode is moved 6.6 mm by the handle of the machine vice. The compiled LabVIEW platform performs the correlation peak and the displacement calculation of the barcode. The green and red curves represent the original correlation peak curve and the real-time correlation peak curve, respectively. The identified displacement is 6.6 mm. The test result is accurate.

In Cases 2 to 5, the barcode is subjected to various masks in these cases, and the most mask area of the ROI reaches 30%. Cases 2 to 5 are performed based on condition 1, and the movement at this time was still 6.6 mm. After correlation calculations, the test results are still 6.6 mm. The conclusion shows that the partial mask of the ROI does not

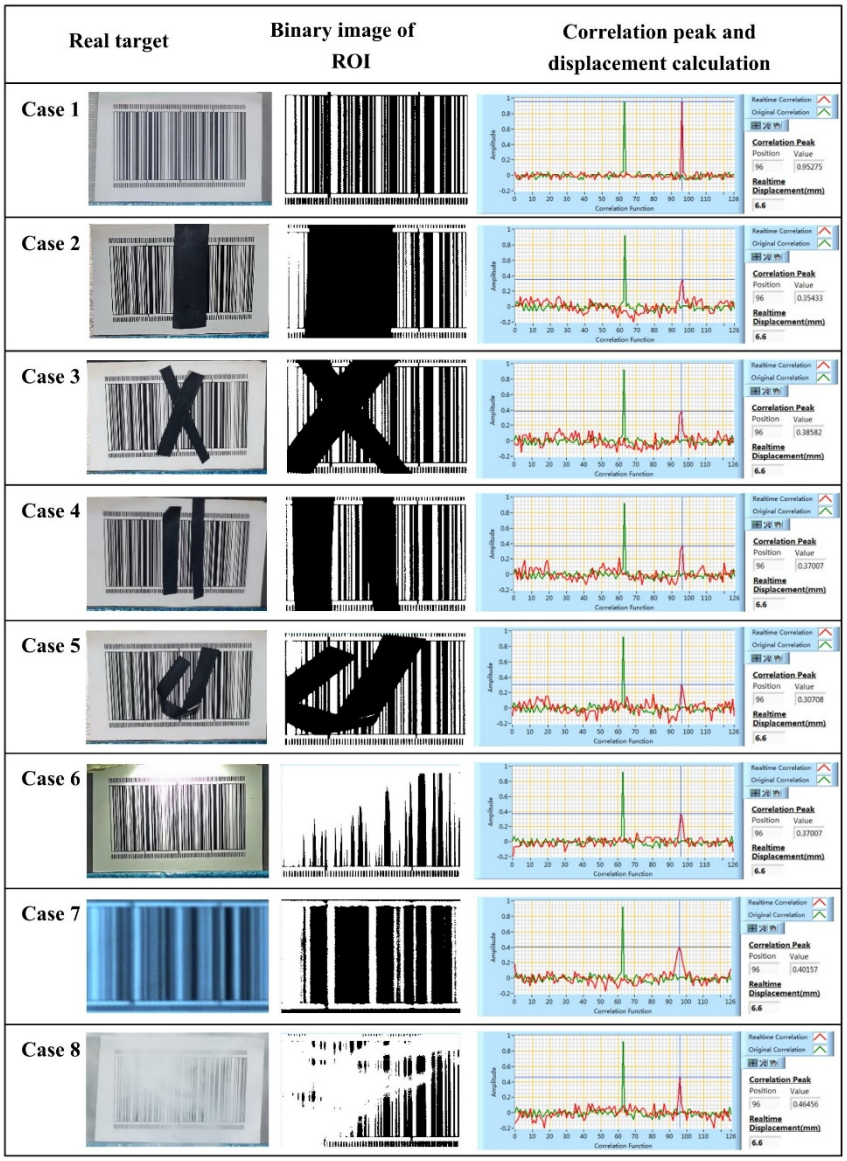

Fig. 12 Anti-interference tests

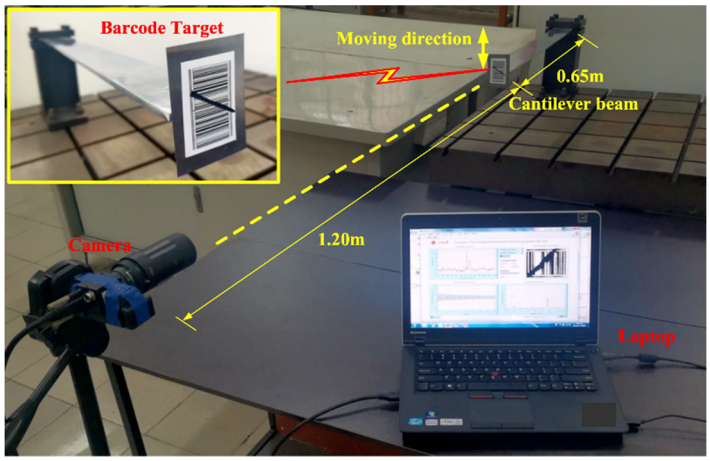

Fig. 13 Dynamic displacement measurement

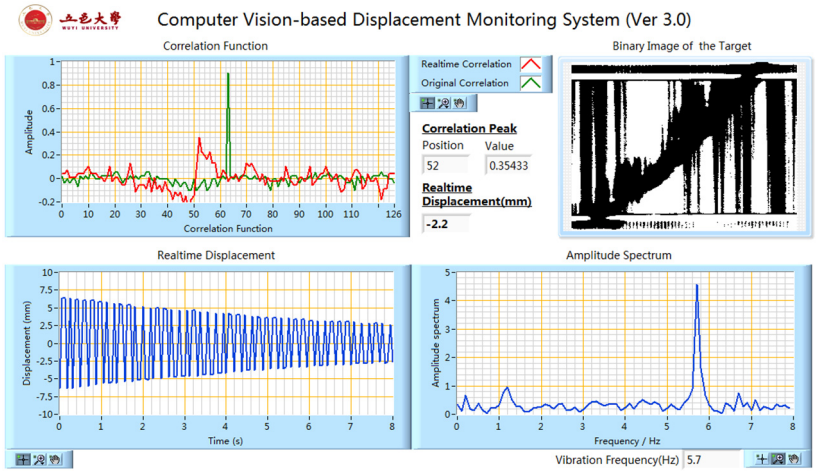

Fig. 14 Dynamic displacement and frequency identification results through the system

affect the accuracy of the measurement results. However, the partial mask of the ROI affects the amplitude of the correlation peak. In the case of no mask, the magnitude of the correlation peak is close to one. When the ROI is partial mask, the amplitude of the correlation peak will decrease as shown in blue cross cursor.

Cases 6 to 8 are uneven illumination, out of focus and smoke effect, respectively. The movement position is no changing in these cases. Although the binary image of ROI has been severely blurred, the displacement corresponding to the correlation peak is still 6.6 mm.

In summary, the m-sequence based visual measurement can ensure the accuracy of the displacement measurement in various harsh environments, such as partial mask, uneven illumination, out of focus and smoke effect. The proposed method and system in this article have a powerful anti-interference performance.

5.3 Dynamic displacement measurement

The dynamic test performance of the system is carried out as shown in Fig. 13. The target barcode is vertically fixed at the end of a cantilever beam. To verify the anti-interference performance of the system, the target is set with irregular mask. The cantilever steel beam is 650 mm long, 60 mm wide and 5 mm thick. The target is 1.2 m away from the camera. The frame rate of the camera is set to 16 frames per second to monitor the dynamic displacement and frequency.

An excitation force is applied to the cantilever beam. The dynamic displacement and frequency identification results are as shown in Fig. 14. The test results show that the displacement of the beam end can still be accurately measured in real-time. The first-order frequency is recognized to be approximately 5.7 Hz.

6. Conclusions

This study presents a novel computer vision-based method for displacement measurement using a new type of m-sequence target. The main contributions of this study are summarized as follows:

(1) The autocorrelation and anti-interference characteristics of m-sequences are confirmed by theoretical derivations. The m-sequence is first applied to the vision-based structural displacement measurement in this article. A system for structural displacement measurement based on LabVIEW platform is developed.

(2) System reliability and anti-interference performance are verified by static and dynamic tests in the laboratory. The test results show that the m-sequence based visual measurement can ensure the accuracy of the displacement measurement in various harsh environments, such as partial mask, uneven illumination, out of focus and smoke effect, even if 30% of the target is masked. The proposed method and system have powerful anti-interference performance and can be adopted in practice.

Acknowledgments

This research was supported by Guangdong Basic and Applied Basic Research Foundation, China (Project No. 2018A030313314); the Wuyi University Fund for Joint Research with Hong Kong and Macao (Project No. 2019WGALH18); the Research Grants Council of the Hong Kong Special Administrative Region, China (Project No. PolyU 152621/16E) and NSFC Joint Research Fund for Overseas and Hong Kong and Macao Scholars (Project No. 51629801).

References

Bao, Y.Q., Tang, Z.Y., Li, H. and Zhang, Y.F. (2019), "Computer vision and deep learning-based data anomaly detection method for structural health monitoring", *Struct. Health Monit.*, **18**(2), 401-421. https://doi.org/10.1177/1475921718757405

Brownjohn, J.M.W. (2006), "Structural health monitoring of civil infrastructure", *Phil. Trans. R. Soc.*, **365**, 589-622. https://doi.org/10.1098/rsta.2006.1925

Busca, G., Cigada, A., Mazzoleni, P. and Zappa, E. (2015), "Vibration monitoring of multiple bridge points by means of a unique vision-based measuring system", *Exp. Mech.*, **54**, 255-271. https://doi.org/10.1007/s11340-013-9784-8

Caetano, E., Silva, S. and Bateira, J. (2011), "A vision system for vibration monitoring of civil engineering structures", *Exp. Tech.* **35**, 74-82. https://doi.org/10.1111/j.1747-1567.2010.00653.x

Casciati, F., Casciati, S., Colnaghi, A., Faravelli, L., Rosadini, L. and Zhu, S. (2019), "Vision-based support in the characterization of superelastic U-shaped SMA elements," *Smart Struct Syst.*, *Int. J.*, **24**(5), 669-681. https://doi.org/10.12989/sss.2019.24.5.641

Catbas, F.N., Zaurin, R., Gul, M. and Gokce, H.B. (2012), "Sensor networks, computer imaging, and unit influence lines for structural health monitoring: case study for bridge load rating", *J. Bridge Eng.*, **17**, 662-670. https://doi.org/10.1061/(ASCE)BE.1943-5592.0000288

Chen, J.G., Davis, A., Wadhwa, N., Durand, F., Freeman, W. and Büyüköztürk, O. (2017), "Video Camera-based vibration measurement for civil infrastructure applications", *J. Infrastruct. Syst.*, **23**(3), B4016013. https://doi.org/10.1061/(ASCE)IS.1943-555X.0000348

Ehrhart, M. and Lienhart, W. (2015), "Monitoring of civil engineering structures using a state-of-the-art image assisted total station", *J. Appl. Geodesy.*, **9**(3), 174-182. https://doi.org/10.1515/jag-2015-0005

Feng, D.M. and Feng, M.Q. (2016), "Vision-based multipoint displacement measurement for structural health monitoring", *Struct. Control Health Monit.*, **23**, 876-890. https://doi.org/10.1002/stc.1819

Feng, D.M. and Feng, M.Q. (2018), "Computer vision for SHM of civil infrastructure: From dynamic response measurement to damage detection - A review", *Eng. Struct.*, **156**, 105-117. https://doi.org/10.1016/j.engstruct.2017.11.018

Feng, D.M., Feng, M.Q., Ozer, E. and Fukuda, Y. (2015), "A Vision-based sensor for noncontact structural displacement measurement", *Sensors*, **15**(7), 16557-16575. https://doi.org/10.3390/s150716557

Guo, J. and Zhu, C. (2016), "Dynamic displacement measurement of large-scale structures based on the Lucas-Kanade template tracking algorithm", *Mech. Syst. Signal. Pr.*, **66-67**, 425-436. https://doi.org/10.1016/j.ymssp.2015.06.004

Hu, Y.D., Hou, R.R., Xia, Q. and Xia, Y. (2019), "Temperature-induced displacement of supertall structures: A case study", *Adv. Struct. Eng.*, **22**(4), 982-996. https://doi.org/10.1177/1369433218795288

Jeon, H., Bang, Y. and Myung, H. (2011), "A paired visual servoing system for 6-DOF displacement measurement of structures", *Smart Mater. Struct.*, **20**, 045019. https://doi.org/10.1088/0964-1726/20/4/045019

Jung, H.J., Lee, J.H. Yoon, S. and Kim, I.H. (2019), "Bridge Inspection and condition assessment using Unmanned Aerial Vehicles (UAVs): Major challenges and solutions from a practical perspective", *Smart Struct. Syst.*, *Int. J.*, **24**(5), 669-681. http://doi.org/10.12989/sss.2019.24.5.669

Khuc, T. and Catbas, F.N. (2017), "Computer vision-based displacement and vibration monitoring without using physical target on structures", *Struct. Infrastruct. Eng.*, **13**, 505-516. https://doi.org/10.1080/15732479.2016.1164729

Kim, K., Kim, J. and Sohn, H. (2016), "Development and full-scale dynamic test of a combined system of heterogeneous laser sensors for structural displacement measurement", *Smart Mater. Struct.*, **25**, 065015. https://iopscience.iop.org/article/10.1088/0964-1726/25/6/065015

Koo, K.Y., Brownjohn, J.M.W., List, D.I. and Cole, R. (2013), "Structural health monitoring of the Tamar suspension bridge", *Struct. Control Health Monit.*, **20**, 609-625. https://doi.org/10.1002/stc.1481

Kuddus, M.A., Li, J., Hao, H., Li, C. and Bi. K.M. (2019), "Target-free vision-based technique for vibration measurements of structures subjected to out-of-plane movements", *Eng. Struct.*, **190**, 210-222. https://doi.org/10.1016/j.engstruct.2019.04.019

Lee, J.H., Ho, H.N., Shinozuka, M. and Lee, J.J. (2012), "An advanced vision-based system for real-time displacement measurement of high-rise buildings", *Smart Mater. Struct.*, **21**, 125019. https://iopscience.iop.org/article/10.1088/0964-1726/21/12/125019

Lee, J., Lee, K.C., Cho, S. and Sim, S.H. (2017), "Computer vision-based structural displacement measurement robust to light-induced image degradation for in-service bridges", *Sensors*, **17**(10), 2317. https://doi.org/10.3390/s17102317

Li, J. and Hao, H. (2016), "Health monitoring of joint conditions in steel truss bridges with relative displacement sensors", *Measurement*, **88**, 360-371. https://doi.org/10.1016/j.measurement.2015.12.009

Olaszek, P. (1999), "Investigation of the dynamic characteristic of bridge structures using a computer vision method", *Measurement*, **25**, 227-236. https://doi.org/10.1016/S0263-2241(99)00006-8

Otsu, N. (1979), "A Threshold Selection Method from Gray-Level Histograms", *IEEE Trans. Syst. Man Cybern*, **9**, 62-66. https://doi.org/10.1109/TSMC.1979.4310076

Ou, J.P. and Li, H. (2010), "Structural health monitoring in mainland china: review and future trends", *Struct. Health Monit.*, **9**(3), 219-231. https://doi.org/10.1177/1475921710365269

Peterson, R.L., Ziemer, R.E. and Borth, D.E. (1995), *Introduction*

to Spread Spectrum Communications, Prentice Hall, Inc.
Ribeiro, D., Calçada, R., Ferreira, J. and Martins, T. (2014), "Non-contact measurement of the dynamic displacement of railway bridges using an advanced video-based system", *Eng. Struct.*, **75**, 164-180. https://doi.org/10.1016/j.engstruct.2014.04.051
Song, Y.Z., Bowen, C.R., Kim, A.H., Nassehi, A., Padget, J. and Gathercole, N. (2014), "Virtual visual sensors and their application in structural health monitoring", *Struct. Health Monit.*, **13**, 251-264. https://doi.org/10.1177/1475921714522841
Spencer, B.F. Jr., Hoskere, V. and Narazaki, Y. (2019), "Advances in Computer Vision-Based Civil Infrastructure Inspection and Monitoring", *Engineering*, **5**(2), 199-222. https://doi.org/10.1016/j.eng.2018.11.030
Welch, T.B., Wright, C.H.G. and Morrow, M.G. (2011), *Real-Time Digital Signal Processing from MATLAB® to C with the TMS320C6x DSPs*, (Second Edition), CRC Press.
Xia, Y., Zhang, P., Ni, Y.Q. and Zhu, H.P. (2014), "Deformation monitoring of a super-tall structure using real-time strain data", *Eng. Struct.*, **67**, 29-38. https://doi.org/10.1016/j.engstruct.2014.02.009
Xia, Q., Cheng, Y.Y., Zhang, J. and Zhu, F.Q. (2017), "In-service condition assessment of a long-span suspension bridge using temperature-induced strain data", *J. Bridge Eng.*, **22**(3), 04016124. https://doi.org/10.1061/(ASCE)BE.1943-5592.0001003
Xia, Q., Liu, S.L. and Zhang, J. (2020), "Temperature analysis of a long-span suspension bridge based on a time-varying solar radiation model", *Smart Struct. Syst., Int. J.*, **25**(1), 23-35. https://doi.org/10.12989/sss.2020.25.1.023
Xu, Y., Brownjohn, J.W.M. and Kong, D. (2018), "A non-contact vision-based system for multipoint displacement monitoring in a cable-stayed footbridge", *Struct. Control Health Monit.*, **25**, e2155. https://doi.org/10.1002/stc.2155
Ye, X.W., Ni, Y.Q., Wai, T.T., Wong, K.Y., Zhang, X.M. and Xu, F. (2013), "A vision-based system for dynamic displacement measurement of long-span bridges: algorithm and verification", *Smart Struct. Syst., Int. J.*, **12**(3-4), 363-379. https://doi.org/10.12989/sss.2013.12.3_4.363
Ye, X.W., Dong, C.Z. and Liu, T. (2016a), "Image-based structural dynamic displacement measurement using different multi-object tracking algorithms", *Smart Struct. Syst., Int. J.*, **17**(6), 935-956. https://doi.org/10.12989/sss.2016.17.6.935
Ye, X.W., Yi, T.H., Dong, C.Z. and Liu, T. (2016b), "Vision-based structural displacement measurement: system performance evaluation and influence factor analysis", *Measurement*, **88**, 372-384. https://doi.org/10.1016/j.measurement.2016.01.024
Yi, T.H., Li, H.N. and Gu, M. (2013), "Experimental assessment of high-rate GPS receivers for deformation monitoring of bridge", *Measurement*, **46**(1), 420-432. https://doi.org/10.1016/j.measurement.2012.07.018
Yoon, H., Elanwar, H., Choi, H., Golparvar-Fard, M. and Spencer, Jr. B.F. (2016), "Target-free approach for vision-based structural system identification using consumer-grade cameras", *Struct. Control Health Monit.*, **23**, 1405-1416. https://doi.org/10.1002/stc.1850
Zhou, X.Q., Xia, Y., Wei, Z.L. and Wu, Q.X. (2012), "A videogrammetric technique for measuring the vibration displacement of stay cables", *Geo Spat. Inf. Sci.*, **15**(2), 135-141. https://doi.org/10.1080/10095020.2012.714105